Amphiphilic Surface Chemistry of Fullerenols Is Necessary for Inhibiting the Amyloid Aggregation of Alpha-Synuclein NACore

Yunxiang Sun[1,2], Aleksandr Kakinen[3], Chi Zhang[2], Ye Yang[4], Ava Faridi[3], Thomas P. Davis,[3,5] Weiguo Cao[4], Pu Chun Ke[3] and Feng Ding[2]*

[1]Department of Physics, Ningbo University, Ningbo, Zhejiang 315211, China
[2]Department of Physics and Astronomy, Clemson University, Clemson, SC 29634, USA
[3]ARC Centre of Excellence in Convergent Bio-Nano Science and Technology, Monash Institute of Pharmaceutical Sciences, Monash University, 381 Royal Parade, Parkville, VIC 3052, Australia
[4]Department of Genetics and Biochemistry, Clemson University, Clemson, SC 29634, USA
[5]Australian Institute for Bioengineering and Nanotechnology, The University of Queensland, Brisbane Qld 4072, Australia

Abstract

Featuring small sizes, caged structures, low cytotoxicity and the capability to cross biological barriers, fullerene hydroxy derivatives named fullerenols have been explored as nanomedicinal candidates for amyloid inhibition. Understanding the surface chemistry effect of hydroxylation extents and corresponding amyloid inhibition mechanisms are necessary for enabling applications of fullerenols and also future designs of nanomedicines in mitigating amyloid aggregation. Here, we investigated effects of $C_{60}(OH)_n$ with n=0-40 on the aggregation of NACore (the amyloidogenic core region of the non-amyloid-β component in α-synuclein), the amyloidogenic core of α-synuclein, by computational simulations, transmission electron microscopy (TEM), Fourier transform infrared (FTIR) spectroscopy, thioflavin-T (ThT) fluorescence kinetics and viability assays. Computationally, NACore assembled into cross-β aggregates via intermediates including β-barrels, postulated as toxic oligomers of amyloid aggregation. Hydrophobic C_{60} preferred to self-assemble, and NACore bound to the surface of C_{60} nano-clusters formed β-sheet rich aggregates – *i.e.*, having little inhibition effect. Amphiphilic $C_{60}(OH)_n$ with n=4-20 displayed significant inhibition effects on NACore aggregation, where hydrogen bonding between hydroxyls and peptide backbones interrupted the formation of β-sheets between peptides adsorbed onto the surfaces of fullerenols or fullerenol nano-assemblies due to hydrophobic interactions. Thus, both cross-β aggregates and β-barrel intermediates were significantly suppressed. With hydroxyls increased to 40, fullerenols became highly hydrophilic with reduced peptide binding and thus an inhibition effect on amyloid aggregation. ThT, FTIR and TEM characterizations of $C_{60}(OH)_n$ with n=0,24,&40 confirmed the computational predictions. Our results and others underscore the importance of amphiphilic surface chemistry and the capability of polar groups in forming hydrogen bonds with peptide backbones to render amyloid inhibition, offering a new insight for *de-novo* design of anti-amyloid inhibitors.

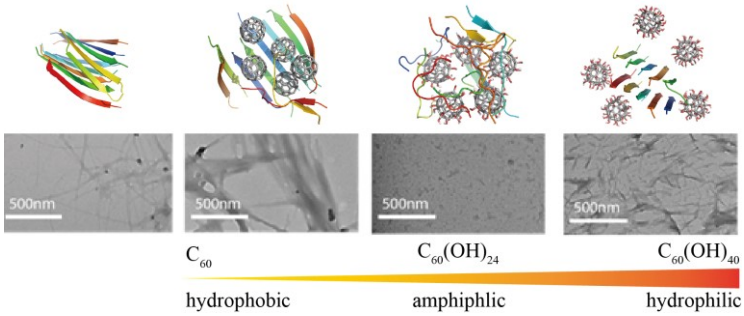

Introduction

Amyloid aggregation of proteins or peptides (e.g., α-synuclein, Aβ, and amylin) is associated with many pathological conditions, including Parkinson's, Alzheimer's diseases and type 2 diabetes[1-3]. In all these diseases, amyloidogenic proteins or peptides independent of their sequences and native structures aggregate into similar fibrillar structures with a common cross-β core, where in-registered β-sheets formed between peptides are aligned perpendicularly to the fibril axis[4-6]. Amyloid cytotoxicity is mainly attributed to the transient, soluble low molecular weight oligomers populated during the aggregation process, although mature fibrils were also reported toxic[7]. Experimental evidence revealed that most cytotoxic aggregation species were β-sheet abundant[8]. Inhibiting amyloid aggregation and especially the population of toxic β-sheet rich intermediates is, therefore, an attractive therapeutic approach against amyloid diseases.

Many small molecular polyphenols, such as curcumin[9, 10], resveratrol[9], and EGCG[11, 12], have been found to have anti-amyloid effects. The capacity of nanoparticles crossing the blood-brain barrier[13] opens new revenues to design anti-amyloid nanomedicine beyond small molecule inhibitors. Various nanoparticles – such as gold nanoparticles[14, 15], fullerene[16, 17], graphene[18], graphene oxide quantum dots[19, 20], hydroxylated carbon nanotubes[21, 22], silica nanohelices [23], polymeric dendrimers[24] and star polymers[25] – have been explored for their effects on modulating amyloid aggregation and mitigating cytotoxicity. Computational studies using molecular dynamics (MD) simulations have also been used to investigate effects of various small molecules[26, 27] and nanoparticles[23, 28] on amyloid aggregation at the molecular and atomic levels. Due to differential interactions of a given inhibitor with various aggregation species, including monomeric peptides, oligomers and final fibrils[13], anti-amyloid effects can be achieved by stabilizing monomers[24], promoting nontoxic off-pathway oligomers[25], or reducing the population of toxic oligomers with accelerated formation of none or less toxic fibrils[29]. Mounting experimental studies established that nanoparticle properties such as size and surface chemistry play important roles in determining the mode and strength of their interactions with proteins[30, 31] and, thus, in modulating amyloid aggregation[14, 32, 33]. Computational studies using simplified models[34, 35] demonstrated that nanoparticles could either promote or inhibit amyloid aggregation depending on binding affinities with amyloid peptides. Since the peptide-binding affinity relies on the surface chemistry of nanoparticles, uncovering the determinant of surface chemistry on amyloid aggregation will be beneficial for the design of future anti-amyloidosis nanoinhibitors.

With features of small sizes, caged structures, low toxicities, and the capability to cross biological barriers[36], fullerene nanoparticles and their derivatives have found numerous biomedical applications[37], including the inhibition of amyloid aggregation[16],[28, 38].

Fullerenols, a class of fullerene derivatives functionalized with hydroxyls (–OH) to increase their solubility and bioavailability[16, 39], are particularly attractive candidates for anti-amyloid inhibitors due to their resemblance of naturally-occurring anti-amyloid polyphenols[33]. Indeed, several studies of fullerenols with certain number hydroxyls have reported inhibition effects on amyloid aggregation of Aβ in Alzheimer's disease and amylin in type 2 diabetes[33, 40]. However, the effect of fullerenol surface chemistry with different extent of hydroxylation on amyloid aggregation remains elusive. In this study, we systematically investigated the surface chemistry effect of fullerenols with different number of hydroxyl groups on the aggregation of NACore, the amyloidogenic core sequence fragment of α-synuclein (residues 68-78， also known as the central hydrophobic core of non-amyloid-β component) in Parkinson's disease[4, 41], by using discrete molecular dynamics simulations (DMD) and complementary transmission electron microscopy (TEM) and a thioflavin-T kinetics assay (ThT). Atomistic DMD simulations - a rapid and accurate MD algorithm widely used to study protein dynamics, protein folding and aggregation[42-47] - have already been used to uncover the effect of fullerenol surface chemistry on the nanoparticle-binding induced impact of protein structures and dynamics[30]. We chose α-synuclein NACore as the model system since the 11-residue fragment is found necessary for the aggregation and cytotoxicity of full-length α-synuclein[48], it has been experimentally shown to form amyloid fibrils with the aggregates displaying high cytotoxicity[41, 49], and importantly the fibril structure has already been determined by X-ray crystallography[41].

We computationally investigated the aggregation of NACore in the absence and presence of fullerene or fullerenols $C_{60}(OH)_n$ with n=0, 4, 8, 12, 16, 20 & 40. Our DMD simulations of NACore aggregation alone recapitulated the cross-β aggregation structure as determined by X-ray crystallography[41]. β-barrel oligomers, recently populated as the toxic oligomers of amyloid aggregation[50] and found as common aggregation intermediates[51, 52], were also observed. In the mixture of fullerenes and NACore, hydrophobic fullerenes self-assembled into nanoclusters while peptides adsorbed on the surfaces of fullerene clusters still formed β-sheet abundant aggregates, suggesting little inhibition effect of insoluble fullerenes on amyloid aggregation in solution. Compared with the purely hydrophobic C_{60}, amphiphilic $C_{60}(OH)_n$ with 4-20 hydroxyls significant inhibited the amyloid aggregation of NACore. The hydrogen bonds between fullerenol hydroxyls and the backbone of the peptide bound to fullerenols or fullerenol clusters interrupted the formation of inter-peptide β-sheets and rendered NACores in coil conformations. Importantly, β-barrel oligomers, observed in the aggregation of pure NACore or with C_{60}, was also significantly reduced. As the number of polar hydroxyl groups further increased, the aggregation inhibition effect of fullerenols started to attenuate due to weaker peptide binding with decreasing hydrophobicity, and $C_{60}(OH)_{40}$ showed no inhibition effect in our simulations. Our complementary ThT and TEM experiments of NACore aggregation in the presence of C_{60}, $C_{60}(OH)_{24}$, and $C_{60}(OH)_{40}$ confirmed that highly hydrophobic C_{60} and highly hydrophilic $C_{60}(OH)_{40}$ had little aggregation inhibition effects, but the amphiphilic $C_{60}(OH)_{24}$ could effectively inhibit NACore from forming amyloid fibrils. Overall our combined computational and experimental studies underscore the amphiphilic surface chemistry and the ability of polar groups to form hydrogen bonds with the peptide backbone to elicit anti-amyloid properties, which may help design novel nanomedicines against amyloid diseases.

Results and discussion

To investigate the effect of fullerenol surface chemistry with different extent of hydroxylation on the amyloid aggregation of NACore, we performed aggregation simulations of peptides (x10) with or without the presence of fullerenes or fullerenols (x5), including C_{60}, $C_{60}(OH)_4$, $C_{60}(OH)_8$, $C_{60}(OH)_{12}$, $C_{60}(OH)_{16}$, $C_{60}(OH)_{20}$, and $C_{60}(OH)_{40}$. For a given molecular system, twenty independent implicit solvent DMD simulations each lasted 200 ns were performed at room temperature by starting from different initial configurations of coordinates and velocities. The equilibration of each system in simulations was assessed according to the time evolution of secondary structure contents, which reached their steady states after 100 ns in all simulations (e.g., representative trajectories of each molecular system were shown in Fig. S1). Hence, we used the last 100 ns trajectories of each independent simulation for data analysis. To validate our computational predictions, complementary TEM and ThT experiments were performed for a set of representative nanoparticles, including hydrophobic C_{60}, amphiphilic $C_{60}(OH)_{24}$ and hydrophilic $C_{60}(OH)_{40}$.

Amphiphilic fullerenols significantly inhibited NACore β-sheet formation. To investigate the inhibition effects of fullerene and fullerenols on the amyloid aggregation of NACore, we first examined the β-sheet propensity of the peptide in our aggregation simulations. As mentioned above, we used the equilibrated last 100 ns trajectories from all independent simulations for the secondary structure analysis. As shown in Fig. 1a, aggregation of NACore alone displayed a high β-sheet propensity, with averaged coil and β-sheet propensities being ~33% and 64%, respectively. The central hydrophobic residues were mostly in β-sheet conformation (Fig. 1b). Peptides in the final aggregates mainly adopted two-layer β-sheets with β-strands in different sheets aligned in parallel (e.g., a representative structure in Fig. 1f), consistent with the experimentally observed cross-β aggregate structure of NACore determined by X-ray crystallography[41].

In the presence of fullerene C_{60}, the β-sheet propensity slightly decreased with overlapping error bars, indicating a weak inhibition effect of C_{60} on the formation of β-sheet rich aggregates, consistent with previous studies of fullerenes interacting with other amyloid peptides[28, 38]. Examination of final aggregates revealed that the fullerenes self-assembled into a single nano-cluster, while NACores adsorbed on the hydrophobic nano-cluster surface still formed inter-peptide β-sheets (Fig. 1g). In contrast, with the modification of adding only 4 hydroxyl groups, $C_{60}(OH)_4$ displayed a significantly inhibition effect for NACore in forming β-sheet rich structures (Fig. 1a,b). As the number of hydroxyl groups increased, the inhibition effect decreased although $C_{60}(OH)_{20}$ still displayed significant inhibition effects comparing to the control of pure NACore aggregation. Similar to C_{60}, these amphiphilic fullerenols with the number of hydroxyls up to 20 also preferred to aggregate into a single nano-cluster, consistent with many experimental reports of large self-assembled nano-clusters in fullerenol suspensions (Fig. 1h-l). Peptides attracted on the nano-cluster surfaces mainly adopted a random coil conformation due to the disruption of hydrogen bonding between the nanoparticles and the peptide backbone, while some small size β-sheets with two or three β-strands were also observed in the case of fullerenols with larger numbers of hydroxyl groups (Fig. 1e-i). Interestingly, the highly hydroxylated $C_{60}(OH)_{40}$ was too hydrophilic to aggregate into nano-clusters as in the cases of hydrophobic and amphiphilic nanoparticles (Fig. 1m), and thus no aggregation inhibition was observed (Fig. 1a,b).

Based on equilibrated trajectories, we also computed the probability distribution function (PDF) of end-to-end distance of each peptide, the distance between Cα atoms of N- and C-terminal residues (Fig. 1c), as well as the total number of inter-peptide hydrogen bonds (Fig. 1d) and between proteins and fullerenols (Fig. 1e). As expected, in the control simulation of NACore

aggregation, the eleven-residue peptide mostly adopted a β-strand conformation with extended end-to-end distance (e.g., a peak of ~3.1 nm in the PDF of Fig. 1c) and formed a large number of inter-peptide hydrogen bonds (e.g., a peak of ~80 hydrogen bonds in Fig. 1d). In the presence of C_{60} molecules, NACores still adopted extend conformations with the peak of the end-to-end distance PDF being ~3.0 nm, and lost some inter-peptide hydrogen bonds due to structural mismatch between the C_{60} nano-cluster and extend β-sheets (Fig. 1g). Amphiphilic fullerenols, on the other hand, rendered NACore peptides less extended (Fig. 1c) as the peptides adsorbed on the surface of fullerenol nano-clusters in bend and coil conformations (Fig. 1a&b), and significantly reduced the number of inter-peptide hydrogen bonds (Fig. 1d) due to the competition of hydrogen bonding between peptides and the hydroxyl groups of the nanoparticles (Fig. 1e). Interestingly, as the number of hydroxyl groups of $C_{60}(OH)_n$ increased till n~16, the total number of peptide-nanoparticle hydrogen bonds initially increased without affecting the number of inter-peptide hydrogen bonds (Fig. 1e), but then started to decrease with the number of inter-peptide hydrogen increasing (i.e., the inhibition effect weakens). With n = 40, the probability distributions of end-to-end distances (Fig. 1c) and the total number inter-chain hydrogen bonds (Fig. 1d) were comparable to these of the control, and the formation of peptide-nanoparticle hydrogen bonds became rare with the PDF peaked around zero (Fig. 1e).

Amphiphilic fullerenols inhibited the population of β-barrel oligomer intermediates. To understand the formation of β-sheet rich oligomers during NACore aggregation, we computed the size distribution of β-sheets (i.e., the number of β-strand forming the sheet), shown in Fig. 2a. In the control simulations, NACore predominantly formed 5- and 10-strand β-sheets. The peak around 5-strand β-sheets corresponded to the two-layer β-sheet structures (Fig. 1c and Fig. 2f,g). The large β-sheets with 8-10 strands in our simulations (with ten peptides) were single β-sheets often in a close form as β-barrels (Fig. 2e&f). This type of β-barrel oligomers formed by amyloidogenic peptides, first structurally-determined from a slow-aggregating αB crystallin fragment[50], has been postulated as the potentially cytotoxic oligomers of amyloid aggregation due to their well-defined structures and compatibility to the "amyloid-pore" hypothesis of toxicity[51, 53, 54]. Possible formation of β-barrel oligomers was also reported in full length Aβ and fragments[52, 55-58]. Recently, our systematic computational studies of multiple amyloidogenic fragments using DMD simulations suggested β-barrel oligomers were common aggregation intermediates towards the formation of cross-β like aggregates[51, 59].

The probability of observing β-barrel oligomers in equilibrated trajectories of each molecular system was computed using a network-based algorithm of identifying β-barrel oligomers as closed β-sheets[42] (Fig. 2b). In control simulations, NACore displayed a high probability to form β-barrels during aggregation (~20%, Fig. 2b). In the presence of C_{60}, we observed reduced population of β-barrel oligomers although the probability of forming large size β-sheet with the number of β-strands 7-10 was increased (Fig. 2a&b). NACore oligomers adsorbed on the surfaces of fullerene nano-clusters formed either single β-sheets (Fig. 2g) or β-barrels (Fig. 2h). In contrast, NACore peptides in the presence of amphiphilic fullerenols - e.g., $C_{60}(OH)_n$ with n up to 20 - only formed small β-sheets with 2-4 strands (Fig. 2a and Fig. 2i) while most peptides did not form β-sheets (i.e., in coil conformations as shown in Fig. 1a and Fig. 2a). As a result, β-barrel oligomers were hardly detected in the presence of fullerenols with n=4-12, although the population of β-barrels increased with increasing hydroxylation levels (Fig. 2b). For instance, β-barrel formation was observed in the $C_{60}(OH)_{16}$ and $C_{60}(OH)_{20}$ (Fig. 2j) systems with a probability of ~1.5% and ~5.4%, respectively. As the number of hydroxyl groups increased to 40, we observed

similar size distributions of β-sheets and population of β-barrels as in the control, suggesting little inhibition effect on NACore aggregation and potential toxicity.

Structural analyses of nanoparticle-peptide complexes revealed the inhibition mechanism. To characterize inter-molecular interactions in the aggregates, we first calculated the residue-wise inter-peptide contact probabilities between main-chain (MC) and side-chain (SC) atoms (Fig. 3 & Fig. S2). NACore, when aggregating alone, formed both parallel and anti-parallel β-sheets with anti-parallel alignments being observed more frequently (e.g., the diagonal pattern in the main-chain contact frequencies of Fig. 3a and snapshots in Fig. 1&2). The high contact frequency between hydrophobic residues indicated the important role of hydrophobic interactions in NACore aggregation. Compared to control simulations, amphiphilic fullerenols significantly reduced inter-peptide interactions between both main-chains and side-chains while hydrophobic C_{60} and hydrophilic $C_{60}(OH)_{40}$ displayed either weak or no inhibition effects on inter-peptide interactions, fully consistent with the secondary structure analysis (Fig. 1a,b).

We further characterized the structural properties of molecular complexes formed between peptides and nanoparticles during aggregation by computing the radial distribution function (RDF) of the peptides or the nanoparticle atoms (Fig. 3b & Fig. S2). When NACores were aggregating in the presence of hydrophobic fullerene or amphiphilic fullerenols, NACore formed stable molecular complexes with nanoparticles located in the interior and peptides in the peripheral (Fig. 3b & Fig. S2). With increasing hydroxylation level, nanoparticles became less compact inside nanoparticle-peptide complexes and proteins started to mix with the more hydrophilic fullerenols indicated by the increased probability of finding protein atoms inside the fullerenol-peptide complexes. In the case of $C_{60}(OH)_{40}$, the highly hydrophilic fullerenols were found outside of peptide assemblies. We also estimated the probability distribution of the peptide backbone or side-chain atoms as a function of their distances to nanoparticles or nanoparticle assemblies (PDF in Fig. 3c), defined as the minimum distance between a peptide atom and any nanoparticle atoms. In the presence of C_{60}, there were two peaks for side-chain atoms, and one peak for main-chain atoms located between the two side-chain peaks. This corresponds to their molecular assemblies (e.g., Fig. 1g, 2g&2h) featuring peptides on the surface forming β-sheets with one side interacting with the hydrophobic surface of C_{60} nano-clusters. Without polar groups forming hydrogen bonds with peptide backbones, C_{60} preferred to interact with the side-chains instead of the backbones of NACore. In contrast, amphiphilic fullerenols could form hydrogen bonds with the peptide backbones and interact with the hydrophobic side-chains of NACore, resulting in similar protein main-chain and side-chain PDFs on their nano-assembly surface. As a result, amphiphilic fullerenols could effectively inhibit the formation of inter-peptide hydrogen bonds and thus β-sheets, hindering amyloid aggregation.

Biophysical experiments confirmed the predicted fibrillization inhibition of NACore by amphiphilic $C_{60}(OH)_{24}$ and little effect by hydrophobic C_{60} and hydrophilic $C_{60}(OH)_{40}$. To validate our computational predictions, ThT assay and TEM imaging were applied to investigate the fibrillization kinetics and morphology of NACore in the absence and presence of hydrophobic C_{60}, amphiphilic $C_{60}(OH)_{24}$ and hydrophilic $C_{60}(OH)_{40}$. Due to the limitation of commercial availability, $C_{60}(OH)_{24}$ was tested as the representative amphiphilic fullerenol. Given the observed trends in our simulations (Fig. 1-3), we expected $C_{60}(OH)_{24}$ having a similar effect on NACore aggregation as that of $C_{60}(OH)_{20}$.

ThT experiments showed that C_{60} had nearly no effects on NACore aggregation kinetics over a wide-range of fullerene concentrations (4 μM, 0.2 mM, & 1 mM in Fig. S3a). $C_{60}(OH)_{24}$ could efficiently inhibit NACore fibrillization at sub-stoichiometry concentrations of 2 and 4 μM by increasing the lag time and reducing the total amyloid after saturation. As the fullerenol concentration increased to an equimolar ratio of 10 μM, the amyloid aggregation was not detected within 36 h (Fig. S3b). $C_{60}(OH)_{40}$ displayed some weak inhibition effect only when its concentration increased to 20 μM or more (Fig. S3c). For comparison, the aggregations kinetics of NACore (10 μM) in the presence of same nanoparticle concentrations (4 μM) was shown in Fig. 4a. The aggregation half-time of NACore at different concentrations of $C_{60}(OH)_{24}$ and $C_{60}(OH)_{40}$ was analyzed in Fig. 4b, showing that $C_{60}(OH)_{24}$ could efficiently inhibit NACore fibrillization at sub-stoichiometry concentrations while the concentration of $C_{60}(OH)_{24}$ had to be up to 100 times in order to observe aggregation inhibition effect. The secondary structure of NACore with and without C_{60}, $C_{60}(OH)_{24}$ and $C_{60}(OH)_{40}$ was further studied by using Fourier transform infrared (FTIR) spectroscopy. The β-strand content for all samples displayed increasing over 48 h of incubation (Fig. 5). However, the increase of β-strands was the least in the presence of $C_{60}(OH)_{24}$ indicating reduced aggregation of NACore. This result is consistent with our simulation data, where the β-sheet content of NACore in the presence of $C_{60}(OH)_{20}$ (~34.2%) was much lower than that in the presence of C_{60} or $C_{60}(OH)_{40}$ (~50.7% and ~65.2%).

TEM imaging confirmed that C_{60} was hydrophobic with a high propensity to agglomerate into micron-sized aggregates while $C_{60}(OH)_{24}$ and $C_{60}(OH)_{40}$ could be suspended in solution without forming large aggregates (Fig.6a-c). NACore alone formed slender fibrils (Fig. 6d&h). In the presence of C_{60}, NACores aggregated around C_{60} clusters forming wide ribbon-like aggregates (Fig. 6e&i). Since the highly hydrophobic fullerene molecules readily formed micron-sized aggregates having limited available surface area for interacting with peptides, C_{60} did not display the weak aggregation inhibition effect as observed *in silico*, where a small number of C_{60} in simulations formed only nano-sized clusters with higher surface-bulk ratio and relatively more active surface for peptide binding. The observation of NACores forming fibrils around C_{60}, likely due to fibril nucleation of peptides adsorbed onto the surface of C_{60} aggregates, is consistent with the observation of NACore β-sheets formed around C_{60} nanoclusters in simulations (Fig. 1-2). As predicted by DMD simulations, $C_{60}(OH)_{24}$ strongly inhibited NACore from forming fibrils (Fig. 6f,j). In the presence of $C_{60}(OH)_{40}$, NACore formed shorter and slightly wider aggregates compared to the control. The experimentally observed aggregation morphology change and the retardation of aggregation at high $C_{60}(OH)_{40}$ concentrations (Fig. 4b & S3) might result from the dynamic and weak hydrogen bonding between $C_{60}(OH)_{40}$ and peptides as revealed in simulations (Fig. 1e). Especially at high concentrations, $C_{60}(OH)_{40}$ effectively slowed down the aggregation kinetics and also allowed the accumulation of more aggregation nucleus.

Both the computational and experimental data reveled that $C_{60}(OH)_{24}$ could effectively inhibit the amyloid fibrillization of NACore. To evaluate whether the inhibition of aggregation could also reduce the cytotoxicity of NACore, the viability of SH-SY5Y neuronal cells exposed to NACore with or without $C_{60}(OH)_{24}$ were performed (Fig. S4). The cell death probability result showed that $C_{60}(OH)_{24}$ had low cytotoxicity itself and could effectively reduce the toxicity of NACore. Since the aggregation inhibition effects of fullerene and its hydroxyl derivatives were studied on NACore, we also tested their effects on the aggregation of full length α-synuclein by the ThT assay (Fig. S5). Similarly, $C_{60}(OH)_{24}$ was the most effective inhibitor of the protein aggregation, whereas $C_{60}(OH)_{40}$ was less effective and C_{60} did not show any effect on the rate of

aggregation (Fig. S5). The amyloid aggregation of full length α-synuclein, especially the formation of soluble oligomers, could cause lipid membrane leakage and cell death[60-62]. Our results also validated the use of NACore as a model system for understanding the aggregation behavior of full length α-synuclein.

Importance of amphiphilic surface chemistry in eliciting inhibition effects on amyloid aggregation. Our computational and experimental results revealed that amphiphilic fullerenols $C_{60}(OH)_n$ with a wide-range of hydroxylation levels (e.g., n=4-24) had significant inhibition effects on amyloid aggregation of NACore, while hydrophobic fullerene or highly hydrophilic fullerenol $C_{60}(OH)_{40}$ had no or weak effects. Many nanoparticle inhibitors reported in literature also feature amphiphilic surface chemistry. For example, amphiphilic graphene oxides and nanocomposites containing graphene oxides were found to inhibit the amyloid aggregation of Aβ[63, 64], amylin[19], and α-synuclein[20]. Complementary to experimental studies, the inhibition mechanisms of these carbon-based amphiphilic nanoparticles were also well studied computationally [21, 22, 28, 65, 66]. In addition, OH-terminated PAMAM dendrimer, an amphiphilic macromolecule, could inhibit amylin aggregation[24]. Anti-amyloid small molecule polyphenols[9], such as curcumin[9, 10], resveratrol[9] and EGCG[11, 12], are also amphiphilic in nature. Overall, these studies support the notion that the amphiphilic surface chemistry is likely necessary for eliciting inhibition effects on amyloid aggregation. Proteins and peptides are intrinsically amphiphilic polymers, the hydrophobic component of amphiphilic inhibitor surface chemistry drives the binding between inhibitors and amyloidogenic peptides and the ability of surface polar groups (such as hydroxyls) forming hydrogen bonds with peptide backbones competes with the formation of inter-peptide hydrogen bonds, thus inhibiting the formation of inter-peptide β-sheets and, subsequently, fibrillization.

Conclusions

We systematically studied the effects of fullerene and its hydroxyl derivatives, $C_{60}(OH)_n$ with n=0-40, on the amyloid aggregation of NACore peptides using atomistic DMD simulations and commentary experimental characterization with TEM, FTIR, viability and ThT. Our computational simulations of NACore aggregation alone recapitulated the formation of cross-β structures as observed in prior X-ray crystallography study[41]. β-barrel oligomers, recently postulated as potentially toxic oligomers [50, 51, 55, 56, 58], were also detected as the aggregation intermediates. The hydrophobic fullerenes preferred to self-assemble into nano-clusters and peptides bound to the nano-cluster surface still formed β-sheet rich aggregates as β-barrel oligomers. Amphiphilic fullerenols with up to ~20 hydroxyl groups displayed significant inhibition effects on NACore aggregation. Amphiphilic fullerenols also formed nano-clusters, but surface hydroxyl groups formed hydrogen bonds with the backbone of peptides bound to the surface, efficiently reducing the formation of inter-peptide hydrogen bonds and thus β-sheets. As a result, the formation of both cross-β and β-barrel structures was strongly inhibited. As the number of hydroxyl group increased up to 40, the hydrophilic $C_{60}(OH)_{40}$ only had weak interactions with the peptides and showed little aggregation inhibition. ThT, FTIR and TEM experiments with C_{60}, $C_{60}(OH)_{24}$ and $C_{60}(OH)_{40}$, representing hydrophobic, amphiphilic and hydrophilic nanoparticles, respectively, confirmed our predictions. Our results, together with prior reports of anti-amyloid nanoparticles [21, 22, 24, 28, 65, 66] and small molecules [9-12] in the literature, underscore the amphiphilic surface chemistry and the ability of polar groups to form hydrogen bonds with the

peptide backbone to elicit anti-amyloid properties, which may help the design of novel theranostics against amyloid diseases.

Materials and methods

Simulation system setup. Our model peptide in this study is a central segment of α-synuclein, residues ^{68}GAVVTGVTAVA^{78} due to its critical role in both the aggregation and cytotoxicity of α-synuclein. In order to investigate the effects of fullerene and its derivatives on NACore amyloid aggregation, eight different systems were well studied, where simulated 10 NACore peptides with/without five fullerene/fullerenol (i.e., C_{60}, $C_{60}(OH)_4$, $C_{60}(OH)_8$, $C_{60}(OH)_{12}$, $C_{60}(OH)_{16}$, $C_{60}(OH)_{20}$, $C_{60}(OH)_{40}$). Both the NACore peptides and fullerene/fullerenol molecules were randomly placed in a 7.0 nm cubic simulation box with the minimum distance between inter-chain molecules of no less than 1.5 nm. The initial conformation of the NACore segments was set as full extended. For each molecular system, 20 independent DMD simulations were performed for 200 ns, with accumulated simulation time of 4 μs, starting with different initial configurations (i.e., orientations, coordinates and velocities).

DMD simulations. All simulations were performed using the discrete molecular dynamics (DMD) algorithm[67]. DMD is a unique type of molecular dynamics algorithm, where the inter-atom interaction potentials are modeled by step functions[44]. Details of DMD simulations were discussed in our prior studies[68]. With significantly enhanced sampling efficiency, DMD was widely used to study protein folding/aggregation[43, 69] and protein-nanoparticle interactions[23]. The units of mass, time, length, and energy used in our all-atom with implicit water model were 1 Da, ~50 femtosecond, 1 Å, and 1 kcal/mol, respectively. The temperature of the system was maintained at 300 K using the Anderson's thermostat. In all cases, the peptide concentration was kept around 48 mM.

Computational Analysis. The secondary structure was calculated using the DSSP program[70]. Similar to prior simulation studies, a hydrogen bond was considered to be formed if the distance between the backbone N and O atoms was ≤3.5 Å and the angle of NH···O ≥ 120°[71]. Inter-chain peptide interactions were analyzed by the residue-residue contact frequency. Here, a pairwise residue contact was defined when the distance between the heavy atoms of two non-sequential residues was <0.65 nm. Two chains were considered to form a β-sheet if (i) at least two consecutive residues in each chain adopted the β-strand conformation and (ii) formed at least two backbone hydrogen bonds. If each peptide was connected by two β-sheet neighbors and formed a closed cycle oligomer, this oligomer was treated as a β-barrel structure[42]. The radial distribution function $g(r)$ of atom in each system corresponding to the complex center was calculated by the following equation $g(r)=N_{r,r+dr}/(4\pi r^2 dr)$, where $N_{r,r+dr}$ is the number of atoms within distances of r and $r+dr$ away from the center of the complex.

Experimental preparation of NACore and fullerene/fullerenol. NACore peptide, with sequence GAVVTGVTAVA, was synthesized and HPLC purified by GenScript. Full-length α-synuclein was purchased from AlexoTech (Purity 95% HPLC). The fullerene C_{60} (Cat No. MT-60-2) and fullerenol $C_{60}(OH)_{24}(ONa)_4$ (Cat No. FI-06-02) were purchased from Materials Technologies Research Ltd. The fullerenol $C_{60}(OH)_{40}$ (Cat No. 793248) was purchased from Sigma-Aldrich Co. LLC. The lyophilized powder of NACore peptide was first solubilized in 100%

hexafluorosiopropanol (HFIP) (Sigma) at ~1 mM and sonicated at 30% power efficiency for 30s (Qsonica Q125) to break preformed aggregation. The concentration was then determined spectrophotometrically using a calculated extinction coefficient at 280 nm. Lyophilized α-synuclein was reconstituted in Milli-Q water.

Thioflavin-T Fluorescence Assay. The kinetics of NACore and α-synuclein aggregation were monitored by using the dye Thioflavin T (ThT), the fluorescence of which was dependent on the formation of amyloid fibrils. To initiate fiber formation, the NACore peptide stock was diluted to a final concentration of 10 μM in 100 mM HEPEs (pH 7.4), and 20 μM ThT (Sigma), and varying concentrations of fullerene/fullerenol. All buffers were passed through a HiTrap Chelating HP Column (GE Healthcare) to remove trace amounts of endogenous divalent cations. For α-synuclein kinetics assay the protein was diluted to a final concentration of 50 μM, and ThT concentration in the assay was 50 μM. The assays were performed in sealed Corning 96-well flat bottom, nonbinding surface plates (black), and measured by exciting the ThT in samples at 440 nm and reading the emission at 485 nm at a constant temperature of 37 °C using BioTek Synergy H1 Hybrid Reader with continuous shaking at 425 cpm between measurements.

Transmission electron microscopy. All samples were sonicated at 30% power efficiency for 30s to break preformed aggregation before mixing. Each sample contained 20 μg/mL NACore peptide and with/without 20 μg/mL fullerene/fullerenol respectively, incubated at 37 °C for 24 h absorbed onto 200-mesh formvar/carbon-coated copper grids. TEM images were acquired using a Hitachi H-7600 transmission electron microscope at 100 kV.

Fourier transform infrared (FTIR) spectroscopy. The FTIR spectra of NACore were obtained using a Shimadzu IRTracer-100 spectrophotometer. For this, 5 μL of 100 μM NACore with and without C_{60}, $C_{60}(OH)_{24}$ and $C_{60}(OH)_{40}$ (100 μM) from 0 to 48 h of incubation time were placed on a sample holder, air dried, and their spectra were acquired between 600 and 4,000 cm^{-1} at 20 °C with resolution of 4 cm^{-1}. A blank spectrum was acquired and subtracted from the sample spectra. Peak fitting and secondary structure analysis were performed using PeakFit v4.12 (SeaSolve Software Inc.).

Cell culture and viability assay. SH-SY5Y neuronal cells were cultured in Dulbecco's Modified Eagle Medium: Nutrient Mixture F-12 (DMED-F12, purchased from ATCC) with 10% fetal bovine serum (FBS). A black clear bottom Costar 96-well plate was coated with poly-L-lysine for 30 min at 37 °C and 5% CO_2 to enhance cell adhesion. After washing the wells with PBS, ~50,000 cells were added to each well. The cells were incubated at 37 °C and 5% CO_2 to reach ~80% confluency. The DMED-F12 was then refreshed with 1 μM PI dye in DMEM-F12 and incubated for 30 min. The cells were treated with 100 μM of NACore with and without $C_{60}(OH)_{24}$ (in three different concentrations of 5, 15 and 25 μM). Untreated cells were recorded as controls. All samples were examined in triplicate. The results were measured by Operetta (PerkinElmer, 20× PlanApo microscope objective, numerical aperture NA=0.7) in a live cell chamber (37 °C, 5% CO_2) after 24 h of treatment. The percentage of dead cells (PI-positive) relative to total cell count was determined by a built-in bright-field mapping function of Harmony High-Content Imaging and Analysis software (PerkinElmer).

Supporting Information
Supplementary Figures S1-S5 (PDF)

Author Information
Corresponding authors
*E-mail: fding@clemson.edu

Acknowledgement
This work was supported in part by NSF CBET-1553945 (Ding), NIH R35GM119691 (Ding), and KC Wong Magna Foundation in Ningbo University (Sun). The content is solely the responsibility of the authors and does not necessarily represent the official views of the NIH and NSF.

References

[1] A.M. Morris, R.G. Finke, Alpha-synuclein aggregation variable temperature and variable pH kinetic data: a re-analysis using the Finke-Watzky 2-step model of nucleation and autocatalytic growth, Biophysical chemistry, 140 (2009) 9-15.
[2] A.K. Buell, C. Galvagnion, R. Gaspar, E. Sparr, M. Vendruscolo, T.P. Knowles, S. Linse, C.M. Dobson, Solution conditions determine the relative importance of nucleation and growth processes in alpha-synuclein aggregation, Proceedings of the National Academy of Sciences of the United States of America, 111 (2014) 7671-7676.
[3] P.C. Ke, M.A. Sani, F. Ding, A. Kakinen, I. Javed, F. Separovic, T.P. Davis, R. Mezzenga, Implications of peptide assemblies in amyloid diseases, Chemical Society reviews, 46 (2017) 6492-6531.
[4] M.D. Tuttle, G. Comellas, A.J. Nieuwkoop, D.J. Covell, D.A. Berthold, K.D. Kloepper, J.M. Courtney, J.K. Kim, A.M. Barclay, A. Kendall, W. Wan, G. Stubbs, C.D. Schwieters, V.M. Lee, J.M. George, C.M. Rienstra, Solid-state NMR structure of a pathogenic fibril of full-length human alpha-synuclein, Nature structural & molecular biology, 23 (2016) 409-415.
[5] J.X. Lu, W. Qiang, W.M. Yau, C.D. Schwieters, S.C. Meredith, R. Tycko, Molecular Structure of beta-Amyloid Fibrils in Alzheimer's Disease Brain Tissue, Cell, 154 (2013) 1257-1268.
[6] Y.L. Xiao, B.Y. Ma, D. McElheny, S. Parthasarathy, F. Long, M. Hoshi, R. Nussinov, Y. Ishii, A beta(1-42) fibril structure illuminates self-recognition and replication of amyloid in Alzheimer's disease, Nature structural & molecular biology, 22 (2015) 499-U497.
[7] K.M. Danzer, D. Haasen, A.R. Karow, S. Moussaud, M. Habeck, A. Giese, H. Kretzschmar, B. Hengerer, M. Kostka, Different species of alpha-synuclein oligomers induce calcium influx and seeding, J Neurosci, 27 (2007) 9220-9232.
[8] S. Chimon, M.A. Shaibat, C.R. Jones, D.C. Calero, B. Aizezi, Y. Ishii, Evidence of fibril-like beta-sheet structures in a neurotoxic amyloid intermediate of Alzheimer's beta-amyloid, Nature structural & molecular biology, 14 (2007) 1157-1164.
[9] P. Nedumpully-Govindan, A. Kakinen, E.H. Pilkington, T.P. Davis, P. Chun Ke, F. Ding, Stabilizing Off-pathway Oligomers by Polyphenol Nanoassemblies for IAPP Aggregation Inhibition, Sci Rep, 6 (2016) 19463.
[10] F. Yang, G.P. Lim, A.N. Begum, O.J. Ubeda, M.R. Simmons, S.S. Ambegaokar, P.P. Chen, R. Kayed, C.G. Glabe, S.A. Frautschy, G.M. Cole, Curcumin inhibits formation of amyloid beta oligomers and fibrils, binds plaques, and reduces amyloid in vivo, The Journal of biological chemistry, 280 (2005) 5892-5901.
[11] J. Bieschke, J. Russ, R.P. Friedrich, D.E. Ehrnhoefer, H. Wobst, K. Neugebauer, E.E. Wanker, EGCG remodels mature alpha-synuclein and amyloid-beta fibrils and reduces cellular toxicity, Proceedings of the National Academy of Sciences of the United States of America, 107 (2010) 7710-7715.

[12] D.E. Ehrnhoefer, J. Bieschke, A. Boeddrich, M. Herbst, L. Masino, R. Lurz, S. Engemann, A. Pastore, E.E. Wanker, EGCG redirects amyloidogenic polypeptides into unstructured, off-pathway oligomers, Nature structural & molecular biology, 15 (2008) 558-566.
[13] B. Wang, E.H. Pilkington, Y.X. Sun, T.P. Davis, P.C. Ke, F. Ding, Modulating protein amyloid aggregation with nanomaterials, Environ Sci-Nano, 4 (2017) 1772-1783.
[14] Y.H. Liao, Y.J. Chang, Y. Yoshiike, Y.C. Chang, Y.R. Chen, Negatively Charged Gold Nanoparticles Inhibit Alzheimer's Amyloid-beta Fibrillization, Induce Fibril Dissociation, and Mitigate Neurotoxicity, Small, 8 (2012) 3631-3639.
[15] Q.Q. Ma, G.H. Wei, X.J. Yang, Influence of Au nanoparticles on the aggregation of amyloid-beta-(25-35) peptides, Nanoscale, 5 (2013) 10397-10403.
[16] J.E. Kim, M. Lee, Fullerene inhibits beta-amyloid peptide aggregation, Biochem Bioph Res Co, 303 (2003) 576-579.
[17] Y. Ishida, T. Fujii, K. Oka, D. Takahashi, K. Toshima, Inhibition of Amyloid beta Aggregation and Cytotoxicity by Photodegradation Using a Designed Fullerene Derivative, Chem-Asian J, 6 (2011) 2312-2315.
[18] Z.X. Yang, C.C. Ge, J.J. Liu, Y. Chong, Z.L. Gu, C.A. Jimenez-Cruz, Z.F. Chai, R.H. Zhou, Destruction of amyloid fibrils by graphene through penetration and extraction of peptides, Nanoscale, 7 (2015) 18725-18737.
[19] M.Y. Wang, Y.X. Sun, X.Y. Cao, G.T. Peng, I. Javed, A. Kakinen, T.P. Davis, S.J. Lin, J.Q. Liu, F. Ding, P.C. Ke, Graphene quantum dots against human IAPP aggregation and toxicity in vivo, Nanoscale, 10 (2018) 19995-20006.
[20] D. Kim, J.M. Yoo, H. Hwang, J. Lee, S.H. Lee, S.P. Yun, M.J. Park, M. Lee, S. Choi, S.H. Kwon, S. Lee, S.H. Kwon, S. Kim, Y.J. Park, M. Kinoshita, Y.H. Lee, S. Shin, S.R. Paik, S.J. Lee, S. Lee, B.H. Hong, H.S. Ko, Graphene quantum dots prevent alpha-synucleinopathy in Parkinson's disease, Nat Nanotechnol, 13 (2018) 812-818.
[21] Y.X. Mo, S. Brahmachari, J.T. Lei, S. Gilead, Y.M. Tang, E. Gazit, G.H. Wei, The Inhibitory Effect of Hydroxylated Carbon Nanotubes on the Aggregation of Human Islet Amyloid Polypeptide Revealed by a Combined Computational and Experimental Study, Acs Chem Neurosci, 9 (2018) 2741-2752.
[22] F. Liu, W. Wang, J. Sang, L. Jia, F. Lu, Hydroxylated Single-Walled Carbon Nanotubes Inhibit Abeta42 Fibrillogenesis, Disaggregate Mature Fibrils, and Protect against Abeta42-Induced Cytotoxicity, Acs Chem Neurosci, (2018).
[23] A. Faridi, Y.X. Sun, Y. Okazaki, G.T. Peng, J. Gao, A. Kakinen, P. Faridi, M. Zhao, I. Javed, A.W. Purcell, T.P. Davis, S.J. Lin, R. Oda, F. Ding, P.C. Ke, Mitigating Human IAPP Amyloidogenesis In Vivo with Chiral Silica Nanoribbons, Small, 14 (2018).
[24] E.N. Gurzov, B. Wang, E.H. Pilkington, P.Y. Chen, A. Kakinen, W.J. Stanley, S.A. Litwak, E.G. Hanssen, T.P. Davis, F. Ding, P.C. Ke, Inhibition of hIAPP Amyloid Aggregation and Pancreatic beta-Cell Toxicity by OH-Terminated PAMAM Dendrimer, Small, 12 (2016) 1615-1626.
[25] E.H. Pilkington, M. Lai, X.W. Ge, W.J. Stanley, B. Wang, M.Y. Wang, A. Kakinen, M.A. Sani, M.R. Whittaker, E.N. Gurzov, F. Ding, J.F. Quinn, T.P. Davis, P.C. Ke, Star Polymers Reduce Islet Amyloid Polypeptide Toxicity via Accelerated Amyloid Aggregation, Biomacromolecules, 18 (2017) 4249-4260.
[26] Y. Sun, W. Xi, G. Wei, Atomic-level study of the effects of O4 molecules on the structural properties of protofibrillar Abeta trimer: beta-sheet stabilization, salt bridge protection, and binding mechanism, J Phys Chem B, 119 (2015) 2786-2794.
[27] Y.X. Mo, J.T. Lei, Y.X. Sun, Q.W. Zhang, G.H. Wei, Conformational Ensemble of hIAPP Dimer: Insight into the Molecular Mechanism by which a Green Tea Extract inhibits hIAPP Aggregation, Sci Rep-Uk, 6 (2016).
[28] Y. Sun, Z. Qian, G. Wei, The inhibitory mechanism of a fullerene derivative against amyloid-beta peptide aggregation: an atomistic simulation study, Physical chemistry chemical physics : PCCP, 18 (2016) 12582-12591.
[29] J. Bieschke, M. Herbst, T. Wiglenda, R.P. Friedrich, A. Boeddrich, F. Schiele, D. Kleckers, J.M.L. del Amo, B.A. Gruning, Q.W. Wang, M.R. Schmidt, R. Lurz, R. Anwyl, S. Schnoegl, M. Fandrich, R.F. Frank, B. Reif, S. Gunther, D.M. Walsh, E.E. Wanker, Small-molecule conversion of toxic oligomers to nontoxic beta-sheet-rich amyloid fibrils, Nat Chem Biol, 8 (2012) 93-101.

[30] S. Radic, P. Nedumpully-Govindan, R. Chen, E. Salonen, J.M. Brown, P.C. Ke, F. Ding, Effect of fullerenol surface chemistry on nanoparticle binding-induced protein misfolding, Nanoscale, 6 (2014) 8340-8349.
[31] S.H. Chen, S.G. Kang, J.D. Luo, R.H. Zhou, Charging nanoparticles: increased binding of Gd@C-82(OH)(22) derivatives to human MMP-9, Nanoscale, 10 (2018) 5667-5677.
[32] G.B. Gao, M.X. Zhang, D.J. Gong, R. Chen, X.J. Hu, T.L. Sun, The size-effect of gold nanoparticles and nanoclusters in the inhibition of amyloid-beta fibrillation, Nanoscale, 9 (2017) 4107-4113.
[33] C.Q. Bai, D.D. Lin, Y.X. Mo, J.T. Lei, Y.X. Sun, L.G. Xie, X.J. Yang, G.H. Wei, Influence of fullerenol on hIAPP aggregation: amyloid inhibition and mechanistic aspects, Physical Chemistry Chemical Physics, 21 (2019) 4022-4031.
[34] S. Radic, T.P. Davis, P.C. Ke, F. Ding, Contrasting effects of nanoparticle-protein attraction on amyloid aggregation, RSC advances, 5 (2015) 105498.
[35] R. Vacha, S. Linse, M. Lund, Surface effects on aggregation kinetics of amyloidogenic peptides, J Am Chem Soc, 136 (2014) 11776-11782.
[36] T. Tsuchiya, I. Oguri, Y.N. Yamakoshi, N. Miyata, Novel harmful effects of [60]fullerene on mouse embryos in vitro and in vivo, FEBS letters, 393 (1996) 139-145.
[37] S. Bosi, T. Da Ros, G. Spalluto, M. Prato, Fullerene derivatives: an attractive tool for biological applications, European journal of medicinal chemistry, 38 (2003) 913-923.
[38] L.G. Xie, Y. Luo, D.D. Lin, W.H. Xi, X.J. Yang, G.H. Wei, The molecular mechanism of fullerene-inhibited aggregation of Alzheimer's beta-amyloid peptide fragment, Nanoscale, 6 (2014) 9752-9762.
[39] A.G. Bobylev, A.B. Kornev, L.G. Bobyleva, M.D. Shpagina, I.S. Fadeeva, R.S. Fadeev, D.G. Deryabin, J. Balzarini, P.A. Troshin, Z.A. Podlubnaya, Fullerenolates: metallated polyhydroxylated fullerenes with potent anti-amyloid activity, Organic & biomolecular chemistry, 9 (2011) 5714-5719.
[40] Z. Bednarikova, P.D. Huy, M.M. Mocanu, D. Fedunova, M.S. Li, Z. Gazova, Fullerenol C60(OH)16 prevents amyloid fibrillization of Abeta40-in vitro and in silico approach, Physical chemistry chemical physics : PCCP, 18 (2016) 18855-18867.
[41] J.A. Rodriguez, M.I. Ivanova, M.R. Sawaya, D. Cascio, F.E. Reyes, D. Shi, S. Sangwan, E.L. Guenther, L.M. Johnson, M. Zhang, L. Jiang, M.A. Arbing, B.L. Nannenga, J. Hattne, J. Whitelegge, A.S. Brewster, M. Messerschmidt, B. Boutet, N.K. Sauter, T. Gonen, D.S. Eisenberg, Structure of the toxic core of alpha-synuclein from invisible crystals, Nature, 525 (2015) 486-+.
[42] X. Ge, Y. Sun, F. Ding, Structures and dynamics of beta-barrel oligomer intermediates of amyloid-beta16-22 aggregation, Biochim Biophys Acta, 1860 (2018) 1687-1697.
[43] Y. Sun, B. Wang, X. Ge, F. Ding, Distinct oligomerization and fibrillization dynamics of amyloid core sequences of amyloid-beta and islet amyloid polypeptide, Physical chemistry chemical physics : PCCP, 19 (2017) 28414-28423.
[44] F. Ding, D. Tsao, H.F. Nie, N.V. Dokholyan, Ab initio folding of proteins with all-atom discrete molecular dynamics, Structure, 16 (2008) 1010-1018.
[45] E. Srinivasan, R. Rajasekaran, Cysteine to Serine Conversion at 111th Position Renders the Disaggregation and Retains the Stabilization of Detrimental SOD1 A4V Mutant Against Amyotrophic Lateral Sclerosis in Human-A Discrete Molecular Dynamics Study, Cell biochemistry and biophysics, 76 (2018) 231-241.
[46] E.A. Proctor, N.V. Dokholyan, Applications of Discrete Molecular Dynamics in biology and medicine, Curr Opin Struct Biol, 37 (2016) 9-13.
[47] Y. Wang, S.J. Bunce, S.E. Radford, A.J. Wilson, S. Auer, C.K. Hall, Thermodynamic phase diagram of amyloid-beta (16-22) peptide, Proceedings of the National Academy of Sciences of the United States of America, 116 (2019) 2091-2096.
[48] B.I. Giasson, I.V. Murray, J.Q. Trojanowski, V.M. Lee, A hydrophobic stretch of 12 amino acid residues in the middle of alpha-synuclein is essential for filament assembly, The Journal of biological chemistry, 276 (2001) 2380-2386.
[49] H. Han, P.H. Weinreb, P.T. Lansbury, Jr., The core Alzheimer's peptide NAC forms amyloid fibrils which seed and are seeded by beta-amyloid: is NAC a common trigger or target in neurodegenerative disease?, Chemistry & biology, 2 (1995) 163-169.

[50] A. Laganowsky, C. Liu, M.R. Sawaya, J.P. Whitelegge, J. Park, M.L. Zhao, A. Pensalfini, A.B. Soriaga, M. Landau, P.K. Teng, D. Cascio, C. Glabe, D. Eisenberg, Atomic View of a Toxic Amyloid Small Oligomer, Science, 335 (2012) 1228-1231.
[51] Y.X. Sun, X.W. Ge, Y.T. Xing, B. Wang, F. Ding, beta-barrel Oligomers as Common Intermediates of Peptides Self-Assembling into Cross-beta Aggregates, Sci Rep-Uk, 8 (2018).
[52] Y. Sun, A. Kakinen, Y. Xing, E.H. Pilkington, T.P. Davis, P.C. Ke, F. Ding, Nucleation of beta-rich oligomers and beta-barrels in the early aggregation of human islet amyloid polypeptide, Biochimica et biophysica acta. Molecular basis of disease, 1865 (2019) 434-444.
[53] H. Jang, B. Ma, R. Lal, R. Nussinov, Models of Toxic beta-Sheet Channels of Protegrin-1 Suggest a Common Subunit Organization Motif Shared with Toxic Alzheimer beta-Amyloid Ion Channels, Biophys J, 95 (2008) 4631-4642.
[54] H.A. Lashuel, D. Hartley, B.M. Petre, T. Walz, P.T. Lansbury, Neurodegenerative disease - Amyloid pores from pathogenic mutations, Nature, 418 (2002) 291-291.
[55] J.X. Pan, J. Han, C.H. Borchers, L. Konermann, Structure and Dynamics of Small Soluble A beta(1-40) Oligomers Studied by Top-Down Hydrogen Exchange Mass Spectrometry, Biochemistry-Us, 51 (2012) 3694-3703.
[56] M. Serra-Batiste, M. Ninot-Pedrosa, M. Bayoumi, M. Gairi, G. Maglia, N. Carulla, A beta 42 assembles into specific beta-barrel pore-forming oligomers in membrane-mimicking environments, Proceedings of the National Academy of Sciences of the United States of America, 113 (2016) 10866-10871.
[57] N. Kandel, T.Y. Zheng, Q. Huo, S.A. Tatulian, Membrane Binding and Pore Formation by a Cytotoxic Fragment of Amyloid beta Peptide, J Phys Chem B, 121 (2017) 10293-10305.
[58] T.D. Do, N.E. LaPointe, R. Nelson, P. Krotee, E.Y. Hayden, B. Ulrich, S. Quan, S.C. Feinstein, D.B. Teplow, D. Eisenberg, J.E. Shea, M.T. Bowers, Amyloid beta-Protein C-Terminal Fragments: Formation of Cylindrins and beta-Barrels, J Am Chem Soc, 138 (2016) 549-557.
[59] Y. Sun, A. Kakinen, Y. Xing, P. Faridi, A. Nandakumar, A.W. Purcell, T.P. Davis, P.C. Ke, F. Ding, Amyloid Self-Assembly of hIAPP8-20 via the Accumulation of Helical Oligomers, alpha-Helix to beta-Sheet Transition, and Formation of beta-Barrel Intermediates, Small, 15 (2019) e1805166.
[60] A. Paul, B.D. Zhang, S. Mohapatra, G. Li, Y.M. Li, E. Gazit, D. Segal, Novel Mannitol-Based Small Molecules for Inhibiting Aggregation of alpha-Synuclein Amyloids in Parkinson's Disease, Frontiers in molecular biosciences, 6 (2019) 16.
[61] N. Lorenzen, S.B. Nielsen, A.K. Buell, J.D. Kaspersen, P. Arosio, B.S. Vad, W. Paslawski, G. Christiansen, Z. Valnickova-Hansen, M. Andreasen, J.J. Enghild, J.S. Pedersen, C.M. Dobson, T.P. Knowles, D.E. Otzen, The role of stable alpha-synuclein oligomers in the molecular events underlying amyloid formation, J Am Chem Soc, 136 (2014) 3859-3868.
[62] R. Sharon, I. Bar-Joseph, M.P. Frosch, D.M. Walsh, J.A. Hamilton, D.J. Selkoe, The formation of highly soluble oligomers of alpha-synuclein is regulated by fatty acids and enhanced in Parkinson's disease, Neuron, 37 (2003) 583-595.
[63] M. Mahmoudi, O. Akhavan, M. Ghavami, F. Rezaee, S.M.A. Ghiasi, Graphene oxide strongly inhibits amyloid beta fibrillation, Nanoscale, 4 (2012) 7322-7325.
[64] J.Y. Li, Q.S. Han, X.H. Wang, N. Yu, L. Yang, R. Yang, C. Wang, Reduced Aggregation and Cytotoxicity of Amyloid Peptides by Graphene Oxide/Gold Nanocomposites Prepared by Pulsed Laser Ablation in Water, Small, 10 (2014) 4386-4394.
[65] L. Baweja, K. Balamurugan, V. Subramanian, A. Dhawan, Effect of graphene oxide on the conformational transitions of amyloid beta peptide: A molecular dynamics simulation study, J Mol Graph Model, 61 (2015) 175-185.
[66] P. Nedumpully-Govindan, E.N. Gurzov, P.Y. Chen, E.H. Pilkington, W.J. Stanley, S.A. Litwak, T.P. Davis, P.C. Ke, F. Ding, Graphene oxide inhibits hIAPP amyloid fibrillation and toxicity in insulin-producing NIT-1 cells, Physical Chemistry Chemical Physics, 18 (2016) 94-100.
[67] S. Peng, F. Ding, B. Urbanc, S.V. Buldyrev, L. Cruz, H.E. Stanley, N.V. Dokholyan, Discrete molecular dynamics simulations of peptide aggregation, Phys Rev E, 69 (2004).
[68] I. Javed, Y.X. Sun, J. Adamcik, B. Wang, A. Kakinen, E.H. Pilkington, F. Ding, R. Mezzenga, T.P. Davis, P.C. Ke, Cofibrillization of Pathogenic and Functional Amyloid Proteins with Gold Nanoparticles against Amyloidogenesis, Biomacromolecules, 18 (2017) 4316-4322.

[69] P. Nedumpully-Govindan, F. Ding, Inhibition of IAPP aggregation by insulin depends on the insulin oligomeric state regulated by zinc ion concentration, Sci Rep, 5 (2015) 8240.
[70] W. Kabsch, C. Sander, Dictionary of Protein Secondary Structure - Pattern-Recognition of Hydrogen-Bonded and Geometrical Features, Biopolymers, 22 (1983) 2577-2637.
[71] Y.X. Sun, Z.Y. Qian, C. Guo, G.H. Wei, Amphiphilic Peptides A(6)K and V6K Display Distinct Oligomeric Structures and Self-Assembly Dynamics: A Combined All-Atom and Coarse-Grained Simulation Study, Biomacromolecules, 16 (2015) 2940-2949.

Figures and Captions

Figure 1. Inhibition of NACore β-sheet formation *in silico*. (a) The averaged content of secondary structures including coils, β-sheets, β-bridges and bends from equilibrium simulations. (b) The propensity of each amino acid to form coil and β-sheet conformation. The probability distribution function (PDF) of (c) the end-to-end distance (End2End), (d) the number of inter-chain hydrogen bonds (Hbond), and (e) the number of hydrogen bonds formed with nanoparticles for each peptide. (f-m) Representative snapshot structures of each simulated molecular systems, randomly selected from 20 independent simulation trajectories.

Figure 2. Conformational analysis of β-sheet containing aggregates. The probabilities of (a) different sizes of β-sheets and (b) β-barrels observed in equilibrated simulations for each system. (c-j) Representative β-sheet aggregations are shown, including (c-d) cross-β aggregates and (e-f) β-barrel intermediates in control simulations; (g) open and (h) closed β-sheets formed by peptides in the presence of C_{60}; (i) coil-rich aggregates of NACore in the presence of amphiphilic $C_{60}(OH)_8$, and (j) β-barrels in the presence of more hydrophilic $C_{60}(OH)_{20}$.

Figure 3. Inter-peptide interactions and structural analyses of nanoparticle-peptide complexes. (a) Per residue inter-peptide contact probabilities computed between main-chain (MC) and side-chain (SC) atoms for each molecular system. (b) Radial distribution function (RDF) for both NACore and nanoparticle atoms in nanoparticle-peptide complexes. (c) Probability distribution (PDF) of peptide backbone or side-chain atoms as the function of their distances to nanoparticles or nanoparticle assemblies, defined as the minimum distance of a peptide atom to any nanoparticle atoms. Results for $C_{60}(OH)_8$ and $C_{60}(OH)_{16}$ are shown in Fig. S2.

Figure 4. NACore aggregation kinetics probed by the ThT assay. (a) Aggregation kinetics of 10 μM NACore in the absence and presence of 4 μM fullerene/fullerenol (black, NACore only; red, $C_{60}(OH)_{24}$; blue, $C_{60}(OH)_{24}$; magenta, C_{60};). (b) Half-time ($t_{1/2}$) of NACore aggregation as a function of the fullerenol concentration (red, $C_{60}(OH)_{24}$; blue, $C_{60}(OH)_{24}$) derived from sigmoidal fitting. Error bars represent standard deviations of three independent measurements.

Figure 5. (a) Characterization of NACore secondary structure upon interaction with C_{60}, $C_{60}(OH)_{24}$ and $C_{60}(OH)_{40}$ over time. (b) FTIR spectra indicate decrease in random coils (peak 1640–1648 cm^{-1}) and increase of β strands (peak 1624–1640 cm^{-1}) over 48 h of the incubation.

Figure 6. NACore aggregation morphology probed by TEM imaging. TEM images of (a) hydrophobic C_{60}, (b) amphiphilic $C_{60}(OH)_{24}$ and (c) hydrophilic $C_{60}(OH)_{40}$. NAcore aggregates in the absence (d,h) and presence of (e,i) C_{60}, (f,g) $C_{60}(OH)_{24}$, and (g,k) $C_{60}(OH)_{40}$.

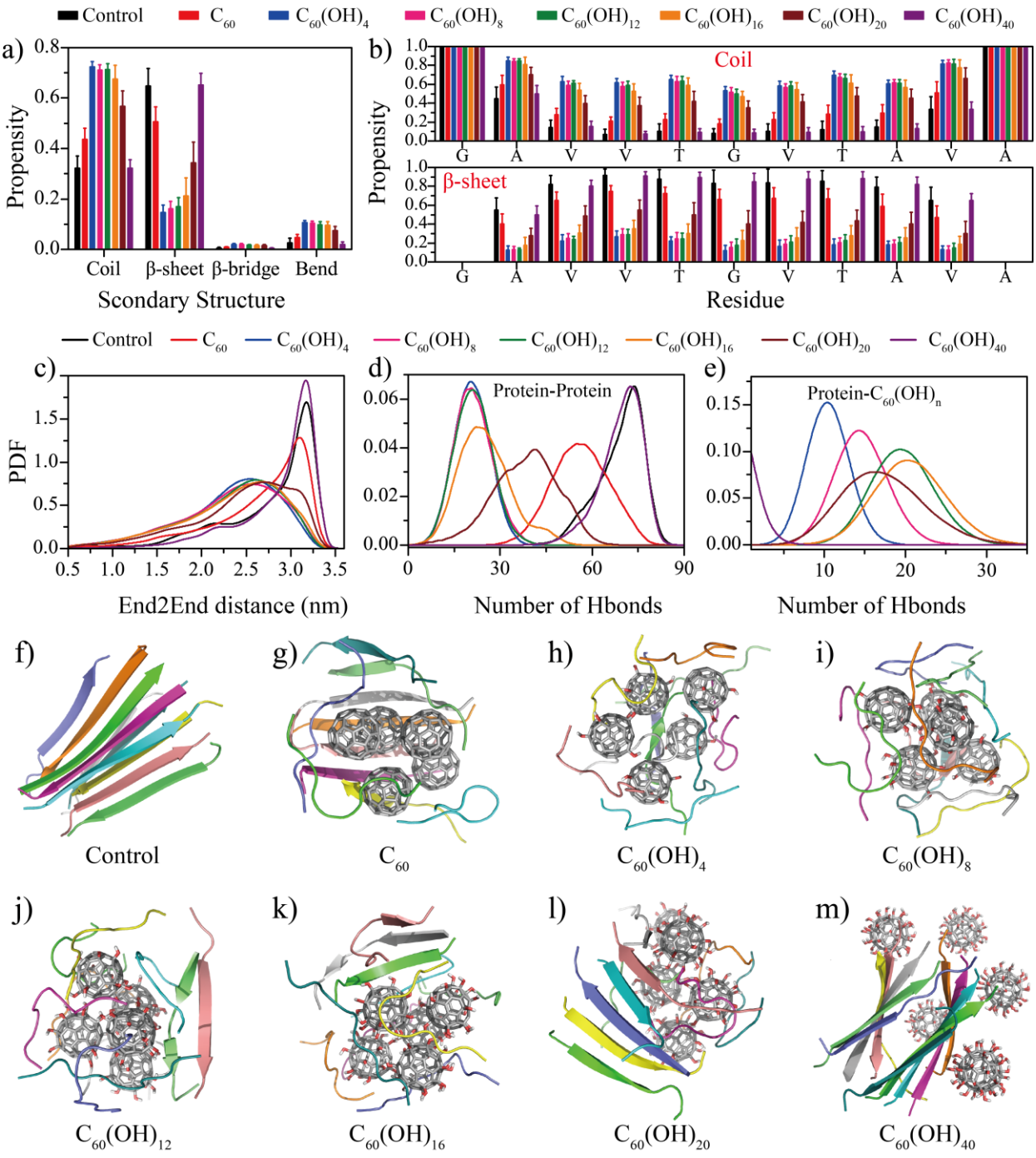
Control
C60
C60(OH)4
C60(OH)8
C60(OH)12
C60(OH)16
C60(OH)20
C60(OH)40
a)
Propensity
Coil
β-sheet
β-bridge
Bend
Scondary Structure
b)
Coil
β-sheet
G A V V T G V T A V A
Residue
c)
PDF
End2End distance (nm)
d)
Protein-Protein
Number of Hbonds
e)
Protein-C60(OH)n
Number of Hbonds
f)
Control
g)
C60
h)
C60(OH)4
i)
C60(OH)8
j)
C60(OH)12
k)
C60(OH)16
l)
C60(OH)20
m)
C60(OH)40

Fig. 1

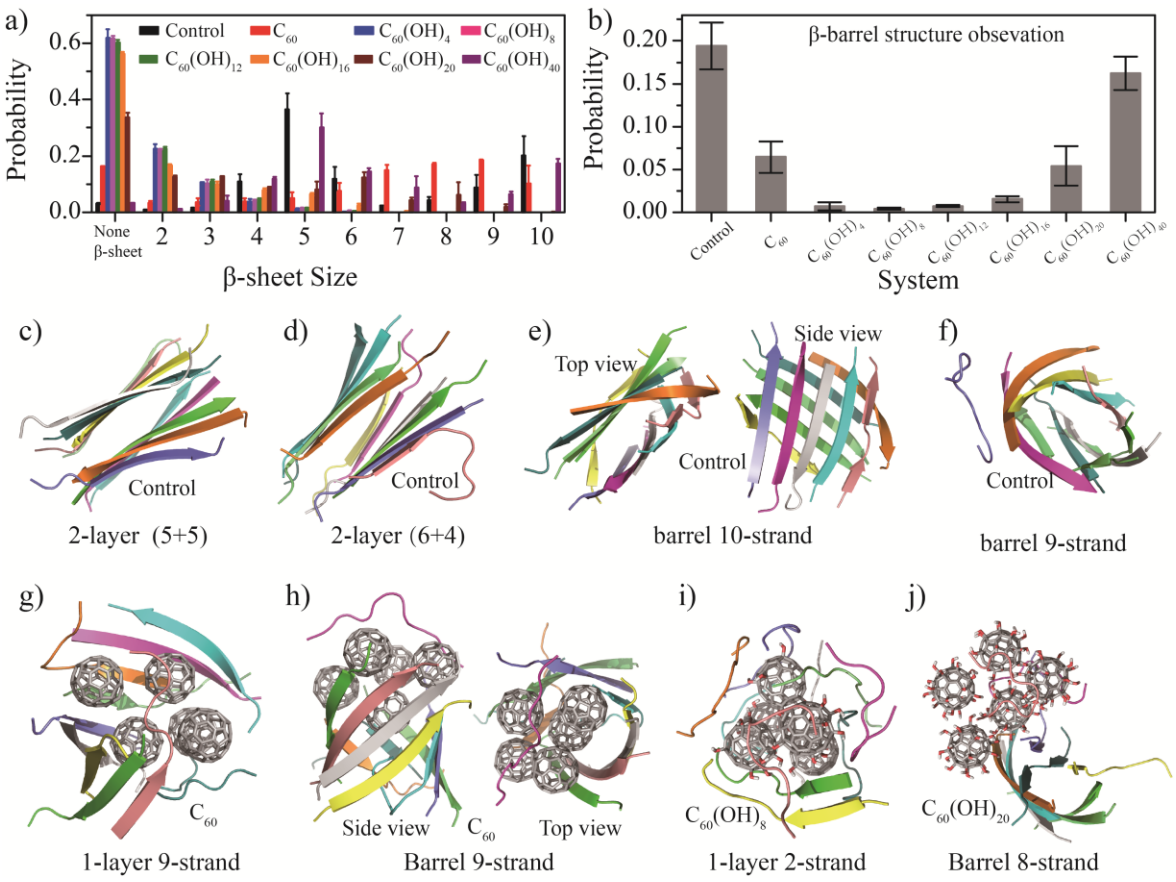
a)
Probability
Control
C60
C60(OH)4
C60(OH)8
C60(OH)12
C60(OH)16
C60(OH)20
C60(OH)40
None β-sheet
β-sheet Size
b)
Probability
β-barrel structure obsevation
Control
C60
C60(OH)4
C60(OH)8
C60(OH)12
C60(OH)16
C60(OH)20
C60(OH)40
System
c)
Control
2-layer (5+5)
d)
Control
2-layer (6+4)
e)
Top view
Side view
Control
barrel 10-strand
f)
Control
barrel 9-strand
g)
C60
1-layer 9-strand
h)
Side view
C60
Top view
Barrel 9-strand
i)
C60(OH)8
1-layer 2-strand
j)
C60(OH)20
Barrel 8-strand

Fig. 2

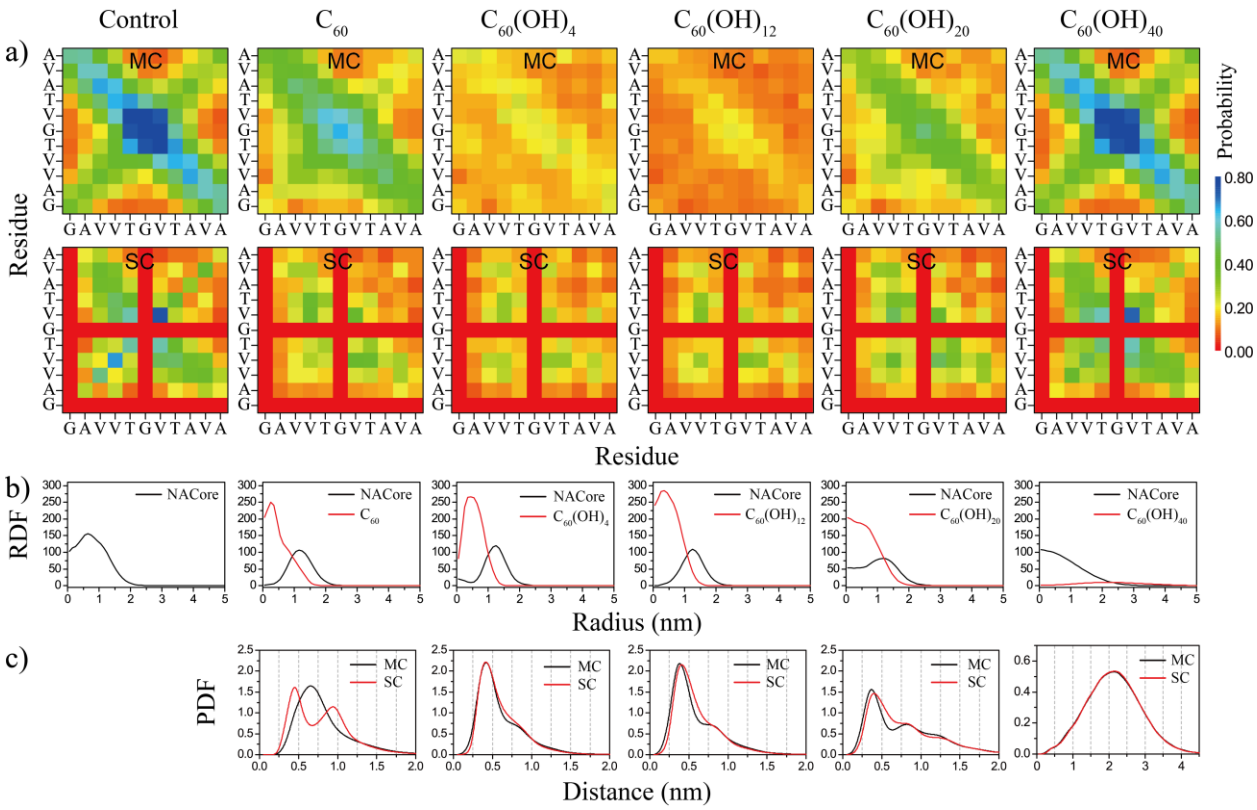
Control
C60
C60(OH)4
C60(OH)12
C60(OH)20
C60(OH)40
a)
MC
SC
Residue
Probability
0.80
0.60
0.40
0.20
0.00
b)
RDF
NACore
Radius (nm)
c)
PDF
MC
SC
Distance (nm)

Fig. 3

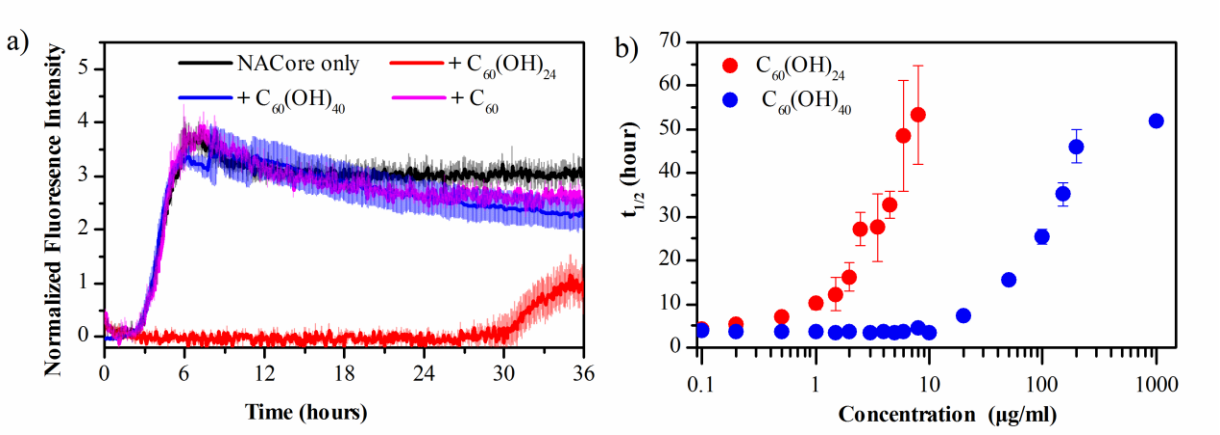
a)
NACore only
+ C60(OH)24
+ C60(OH)40
+ C60
Normalized Fluoresence Intensity
Time (hours)
b)
C60(OH)24
C60(OH)40
t1/2 (hour)
Concentration (μg/ml)

Fig. 4

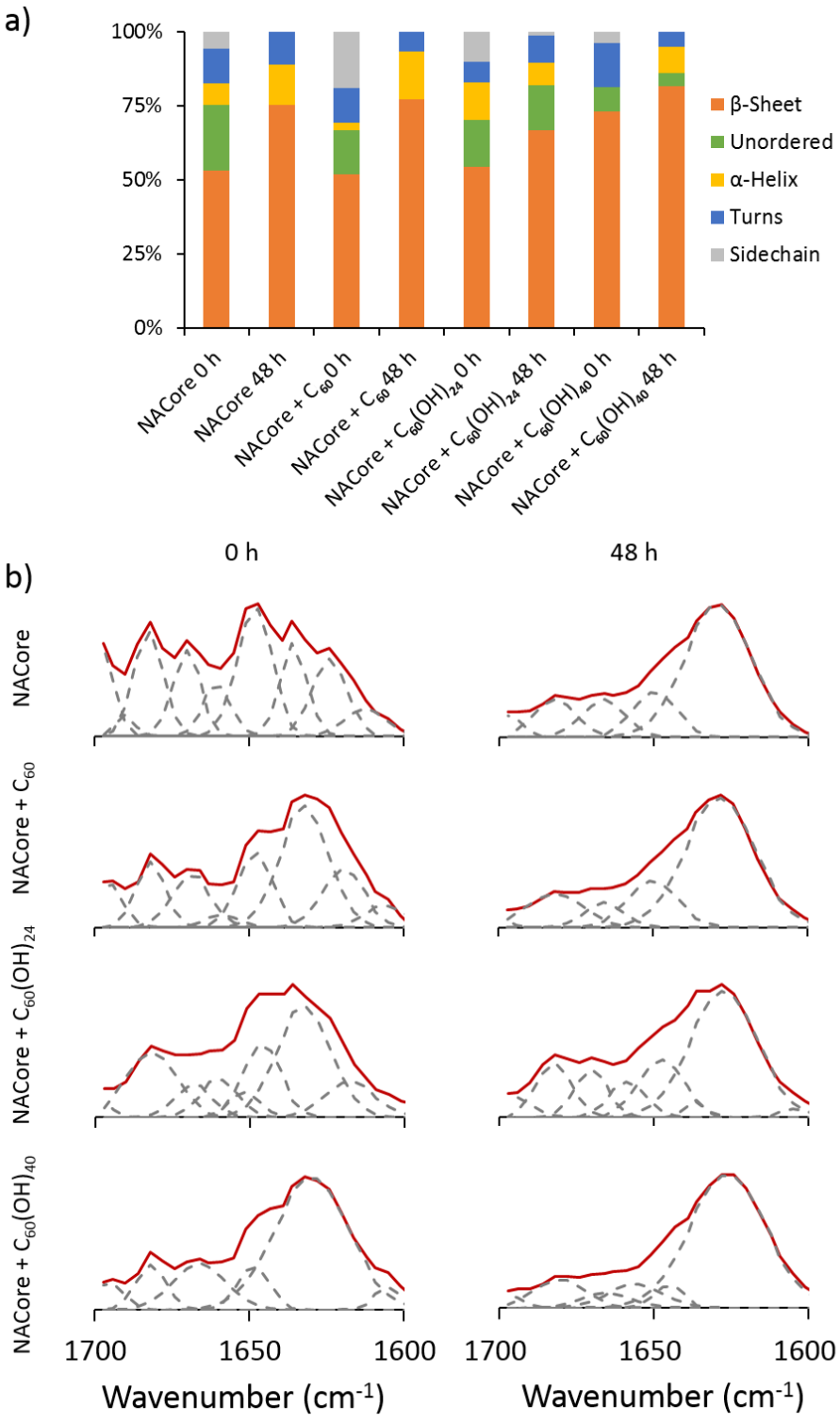
a)
100%
75%
50%
25%
0%
β-Sheet
Unordered
α-Helix
Turns
Sidechain
NACore 0 h
NACore 48 h
NACore + C60 0 h
NACore + C60 48 h
NACore + C60(OH)24 0 h
NACore + C60(OH)24 48 h
NACore + C60(OH)40 0 h
NACore + C60(OH)40 48 h
b)
0 h
48 h
NACore
NACore + C60
NACore + C60(OH)24
NACore + C60(OH)40
1700
1650
1600
Wavenumber (cm-1)

Fig. 5

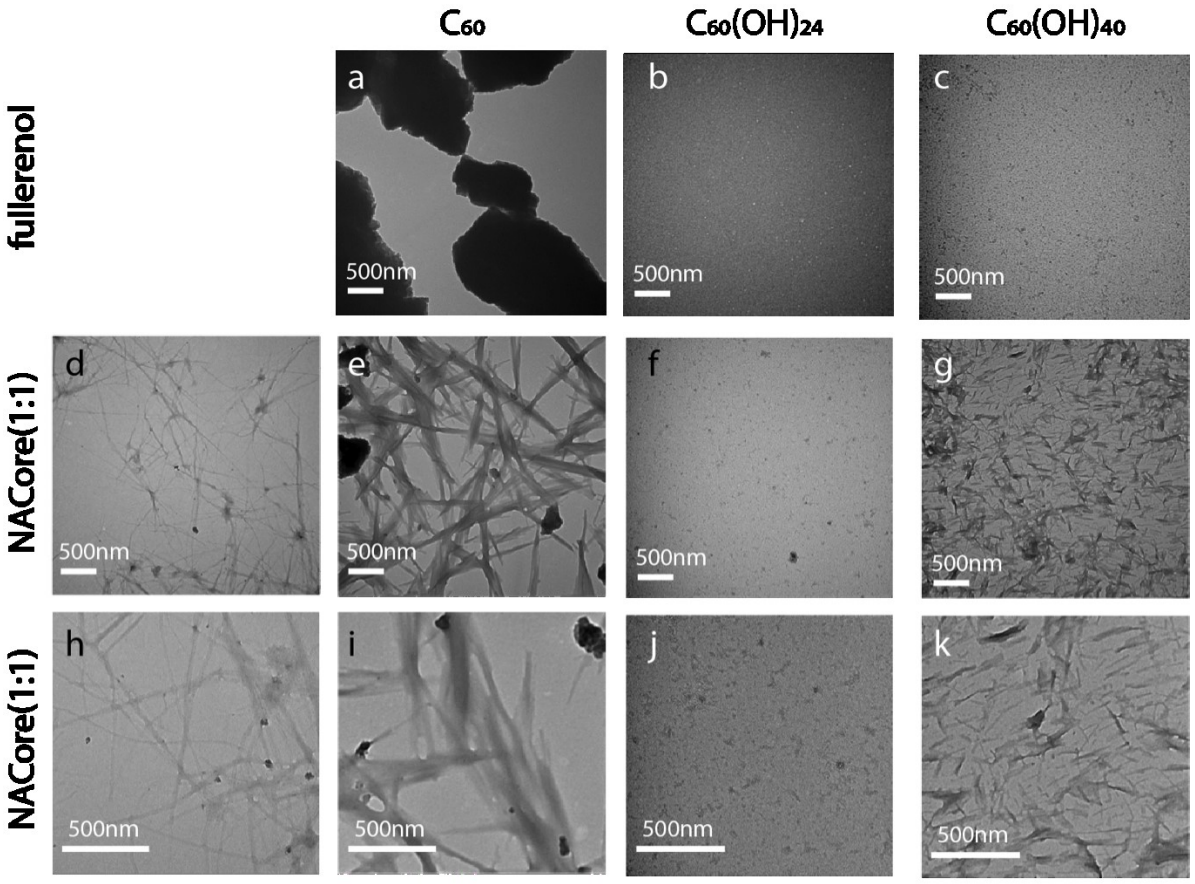
C60
C60(OH)24
C60(OH)40
fullerenol
NACore(1:1)
NACore(1:1)
a
b
c
d
e
f
g
h
i
j
k
500nm

Fig. 6